European Cells and Materials Vol.53 2025 (pages 15–27) DOI: 10.22203/eCM.v053a02 ISSN 1473-2262

Original Article

LGR4 BINDING SMALL RANKL FRAGMENT INHIBITS RANKL-INDUCED BONE RESORPTION

Y. Jang[1,2,3,§], Y.J. Cho[1,2,§], Y. Ko[1,2,3], H. Lee[1,2,3], B. Kim[1,2], C.M. Lee[3,4] and W. Lim[1,2,3,5,*]

[1]Department of Orthopaedic Surgery, Chosun University, 61453 Gwangju, Republic of Korea
[2]Laboratory of Orthopaedic Research, Chosun University, 61453 Gwangju, Republic of Korea
[3]Regional Leading Research Center, Chonnam National University, 59626 Yeosu, Republic of Korea
[4]School of Healthcare and Biomedical Engineering, Chonnam National University, 59626 Yeosu, Republic of Korea
[5]Department of Premedical Program, School of Medicine, Chosun University, 61452 Gwangju, Republic of Korea
[§]These authors contributed equally.

Abstract

Objective: Owing to the crucial role played by the osteoprotegerin-receptor activator of nuclear factor-kappa B-RANK ligand (OPG-RANK-RANKL) triad in osteoclastogenesis, the interaction among these proteins is an attractive target for developing osteoporosis drugs. RANKL binds to leucine-rich repeat containing G protein-coupled receptor 4 (LGR4) comparatively and suppresses the canonical signaling of RANK on osteoclast differentiation. In the present study, we investigated whether a RANKL-derived small peptide, selected based on the binding domain of RANKL with RANK, could lead the inhibition of osteoclast differentiation and activation in the absence of the RANK signal. **Methods:** We introduced small peptides into the RANKL protein based on their binding to LGR4 and investigated whether LGR4-RANKL signaling without RANK-RANKL could inhibit osteoclastogenesis. The binding affinities of RANK-peptides and LGR4-peptides were measured using microscale thermophoresis. The generation and activation of osteoclasts were assessed by tartrate-resistant acid phosphatase (TRAP) staining, bone resorption pit formation, real-time polymerase chain reaction, western blot, and nuclear translocation of nuclear factor of activated T cells (NFATc1) to determine RANKL-derived small peptide. Radiographic and histological analyses were performed to confirm the inhibitory effect on bone resorption in RANKL-induced mice. **Results:** Treatment with a RANKL-derived small peptide led to the binding of LGR4 without binding to RANK, as well as to the inhibition of NFATc1 nucleus translocation through the glycogen synthase kinase-3 beta (GSK-3β) signaling pathway, and showed an inhibition of TRAP activity and decrease of bone resorption in RANKL-induced mice. **Conclusions:** Our study provides a proof of concept that a small fragment of RANKL could be used as a novel therapeutic agent by inhibition of osteoclast through competitive inhibition of RANKL. This study suggests that RANKL-derived small peptides could be used as potential pharmaceutics for the osteoporosis treatment.

Keywords: Bone resorption, TNF superfamily, osteoclast, osteoporosis, RANKL, LGR4.

***Address for correspondence**: W. Lim, Department of Premedical Program, School of Medicine, Chosun University, 61452 Gwangju, Republic of Korea. E-mail: wonbong@chosun.ac.kr.

Introduction

Abnormal bone resorption due to excessive osteoclast activity disrupts the balance in bone remodeling and can lead to severe osteolytic bone diseases, including osteoporosis, osteoarthritis, and metastatic bone tumors [1]. The receptor activator of nuclear factor-kappa B ligand (RANKL) is included in the tumor necrosis factor (TNF) superfamily and plays a pivotal role during differentiation and activation of preosteoclasts [2–4]. Binding of RANKL its receptor activator of nuclear factor-kappa B (RANK) in osteoclast-progenitor macrophages triggers subsequent canonical pathways, including mitogen-activated protein kinase (MAPK), nuclear factor-kappa B (NF-κB), and the nuclear factor of activated T cells (NFATc1) [5–7]. These pathways culminate in the generation and activation of bone-resorbing osteoclasts [8,9]. RANKL can be processed into a soluble form, comprising the signaling, transmembrane, and extracellular domains, which retains its biological activity [3]. While complex gene transfer procedures are necessary to localize the transmembrane domain-containing isoform to the membrane, injection of the truncated soluble form is effective against osteoclast activation in severe bone resorption [10–12]. The molecular structures of RANKL alone and in binding complex with RANK

reveal overall similar architecture that include unique conserved elements conserved receptor binding domain [13, 14]. The mammalian RANKL is a 316-amino acid-long transmembrane protein that includes a receptor-binding C-terminal domain, a hydrophobic transmembrane domain with 20 amino acid sequences, and a relatively long extracellular domain that includes a TNF-homologous region, which serves as an active receptor-binding domain [3]. In murine RANKL, the critical RANK-binding domains are present at positions 180, 189, and 190 on the βA-AA′ loop-βA, and at positions 223 and 224 on the βC-CD loop-βD [15]. In another superfamily member, these domains were known to be lack of intrinsic enzymatic activity and play the role of intracellular signaling conversion to adaptor proteins, leading to the activation of extracellular signal-regulated kinase, c-Jun N-terminal kinase, NF-κB, p38, NFATc1 and protein kinase B (AKT) signaling [16–18].

Currently, the leucine-rich repeat containing G protein-coupled receptor 4 (LGR4) was introduced as another membrane receptor of RANKL [19,20]. In osteoclast precursor cells, RANKL binds to LGR4 comparatively and alleviates the RANK signal on osteoclastogenesis [21]. LGR4 signal leads to the activation of the Gαq and glycogen synthase kinase-3 beta (GSK-3β), which suppresses the transcriptional NFATc1 activation [21]. Additionally, during osteoclastogenesis, signaling cascade of RANKL-RANK-NFATc1 can lead the LGR4 expression, which competes with canonical signaling of RANK by binding of RANKL in differentiation of preosteoclasts [19,22,23]. LGR4 is known to belong to the family of LGR that includes two other members, receptor of follicle-stimulating hormone and thyroid-stimulating hormone, which modulate bone-resorbing activity [24]. In the previous study, based on the study about RANK-binding site on soluble RANKL ectodomains [14], we designed a RANKL-derived variant that can bind to LGR4 rather than RANK. It had been investigated whether this variant could bind to LGR4 but not to RANK, and whether it could inhibit the osteocalstogenesis, resulted in inhibition of bone resorbing activities [25,26]. Our previous results with experimental models of osteoporosis indicated a potentially significant role for the RANKL-derived variant in the relationship between RANKL-LGR4 and RANKL-RANK binding signal.

In this study, we elucidated the therapeutic potential of a small RANKL peptide containing a critical binding site for LGR4. We examined the activities of this peptide to inhibit murine RANKL-induced differentiation and activation of osteoclasts with the aim of developing a treatment for osteoporosis. Additionally, we deciphered the mode of binding to RANKL based on molecular modeling. In this approach, the discovery of a novel small peptide as an inhibitor of RANKL will provide valuable information for the development of antiresorptive therapeutics. The small RANKL fragment described in this study should be a better alternative to the one reported earlier [25,26] because the relatively large size of the latter would limit its clinical applications owing to rapid degradation and the generation of immunogenicity.

Material and Methods

3D Structure Simulation of Small RANKL-Derived Peptide

The full-length RANKL sequence was searched against amino acid sequences in the Protein Data Bank using BLAST. The simulation of the three dimensional (3D) structures of RANKL-derived fragments and template search were performed using Phyre2 (http://www.sbg.bio.ic.ac.uk/~phyre2/html/page.cgi?id=index).

Production of the Small RANKL-Derived Peptides

The complementary DNA (cDNA) for the small RANKL-derived peptide was obtained from Bioneer Co. Ltd. (Daejeon, Republic of Korea). The cDNA was transformed into Escherichia coli BL21-CodonPlus (DE3)-RIPL (69450, Novagen, Carlsbad, CA, USA) and the protein product was obtained as previously described [25,26].

Tartrate-Resistant Acid Phosphatase (TRAP) Activity Assay

For TRAP assay, bone marrow-derived macrophages (BMMs) were isolated by flushing tibial and femoral shafts from mice female Balb/c mice (age, 5 weeks; weight, ~ 25 g; Orient Bio, Inc., Seongnam-si, Republic of Korea) using α-minimal essential medium (α-MEM; 12571063, Invitrogen, Carlsbad, CA, USA). Erythrocytes were removed using Ammonium-Chloride-Potassium (ACK) lysis buffer (A1049201, Gibco, Gaithersburg, MD, USA). The remaining nucleated cells were resuspended in α-MEM supplemented with 10 % fetal bovine serum (A5670701, FBS, Thermo Fisher Scientific Inc., Waltham, MA, USA), 100 U/mL penicillin, and 100 μg/mL streptomycin. To isolate the identified BMMs, cells were incubated for 24 hours with 10 ng/mL macrophage-colony stimulation factor (M-CSF; 416-ML, R&D systems, Minneapolis, MN, USA). Subsequently, non-adherent cells were collected and further cultured with 30 ng/mL M-CSF for 72 hours to induce differentiation into BMMs.

The BMMs were performed with mycoplasma test according to manufacturer's protocol (Takara Bio Inc., Shiga, Japan) and confirmed that the mycoplasma did not exist in all groups (**Supplementary Fig. 1**). The BMMs were plated at a density of 1.4×10^4 cells/well in presence with RANKL-derived fragments at indicated concentration and stained according to previous protocol (**Supplementary Fig. 2**) [25,26].

Bone Resorption Assay

To observe bone resorption *in vitro*, BMMs were cultured with or without the indicated small RANKL peptide according to previous protocol [25,26]. The images of bone resorbing area were acquired using an inverted microscope

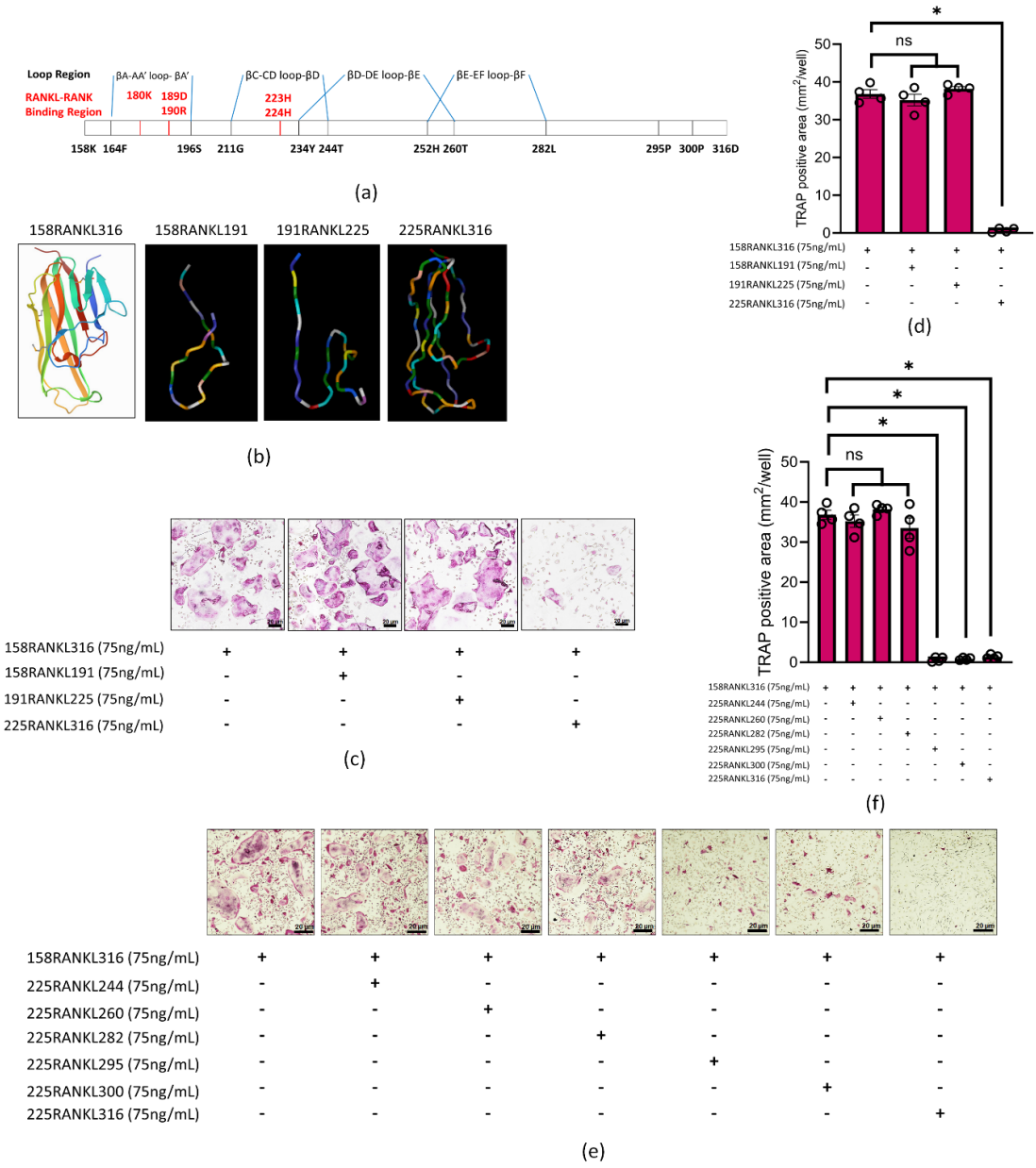

Fig. 1. Classification of RANKL-derived small fragment proteins based on inhibition of osteoclast activation. (**a**) Schematic of the RANKL-derived sequences in our study. (**b**) 3D simulation of RANKL-derived small fragments based on the RANK-binding sequence. (**c**) A representative image of bone marrow-derived macrophages (BMMs) stained for tartrate-resistant acid phosphatase (TRAP; red) following treatment with 158RANKL316 (75 ng/mL), 158RANKL316 (75 ng/mL) + 191RANKL225 (75 ng/mL) and 158RANKL316 (75 ng/mL) + 225RANKL316 (75 ng/mL). Magnification, ×100; scale bar = 20 μm. (**d**) Quantification of TRAP-positive area; Data are presented as the mean ± SD of each data from independent measurements (n = 4). *$p < 0.05$ indicates a significant difference at 158RANKL316 vs. 225RANKL316. ns, not significant. (**e**) A representative image of BMMs stained for TRAP (red) following treatment with 158RANKL316 (75 ng/mL), 158RANKL316 (75 ng/mL) + 225RANKL244 (75 ng/mL), 158RANKL316 (75 ng/mL) + 225RANKL260 (75 ng/mL), 158RANKL316 (75 ng/mL) + 225RANKL282 (75 ng/mL), 158RANKL316 (75 ng/mL) + 225RANKL295 (75 ng/mL), 158RANKL316 (75 ng/mL) + 225RANKL300 (75 ng/mL), and 158RANKL316 (75 ng/mL) + 225RANKL316 (75 ng/mL). Magnification, ×100; scale bar = 20 μm. (**f**) Quantification of TRAP-positive area; Data are presented as the mean ± SD of each data from independent measurements (n = 4). *$p < 0.05$ indicates a significant difference at 158RANKL316 vs. 225RANKL295, 225RANKL300 and 225RANKL316. ns, not significant. RANKL, RANK ligand; RANK, receptor activator of nuclear factor-kappa B; 3D, three dimensional; SD, standard deviation. The 3D simulations were created by Phyre2 (http://www.sbg.bio.ic.ac.uk/~phyre2/html/page.cgi?id=index) and quantified graphs by GraphPad Prism 10 software (https://www.graphpad.com/).

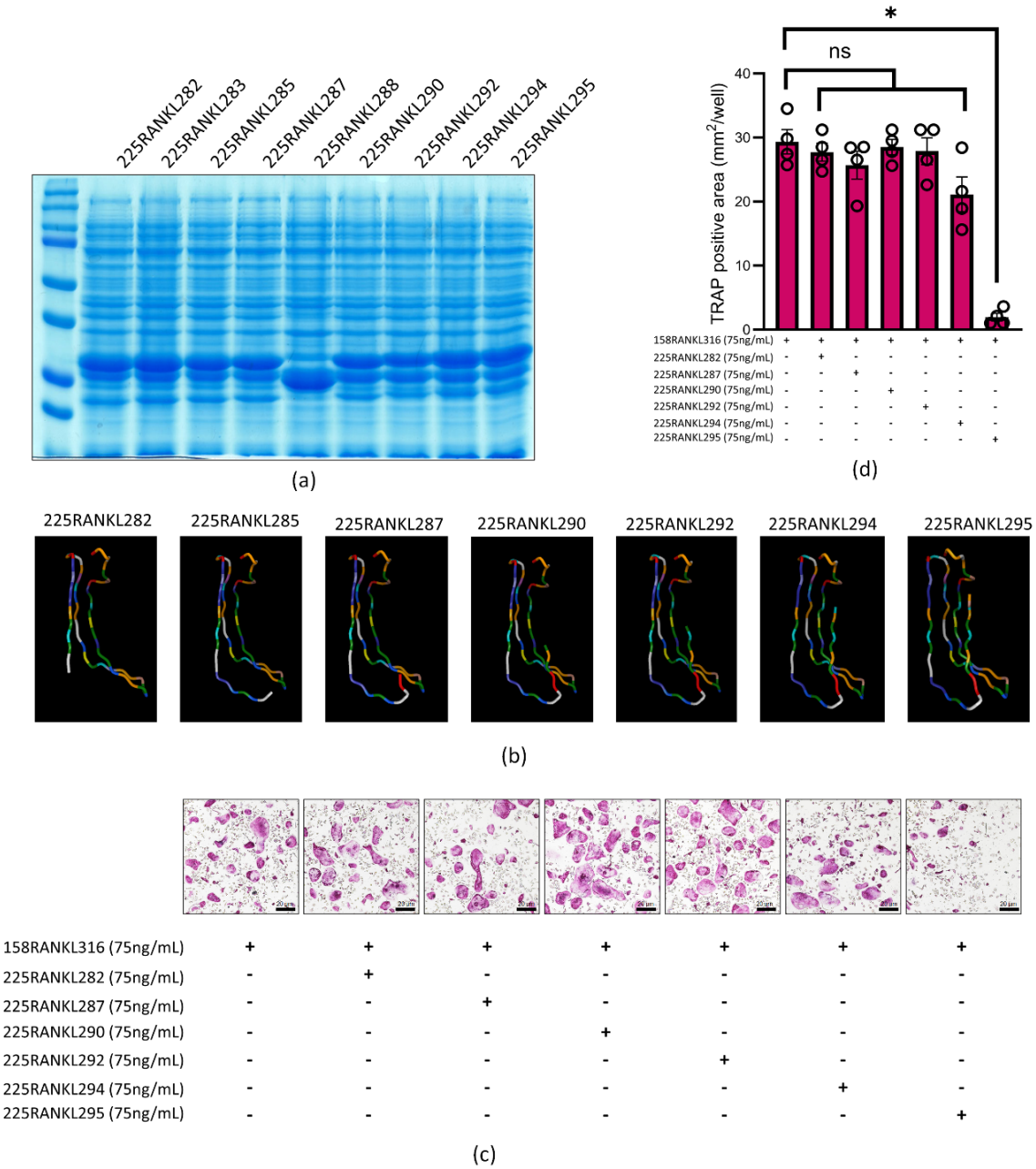

Fig. 2. Selection of RANKL-derived sequential fragment proteins based on inhibition of osteoclast activation. (**a**) SDS-PAGE of fractions in the stepwise purification of RANKL expressed in Escherichia coli upon IPTG induction (lane 1, protein marker; lane 2, 225RANKL282; lane 3, 225RANKL283; lane 4, 225RANKL285; lane 5, 225RANKL287; lane 6, 225RANKL288; lane 7, 225RANKL290; lane 8, 225RANKL292; lane 9, 225RANKL294; lane 10, 225RANKL295). (**b**) 3D simulation of RANKL-derived sequential fragment proteins based on RANK-binding sequence. (**c**) A representative image of bone marrow-derived macrophages (BMMs) stained for tartrate-resistant acid phosphatase (TRAP; red) following treatment with 158RANKL316 (75 ng/mL), 158RANKL316 (75 ng/mL) + 225RANKL282 (75 ng/mL), 158RANKL316 (75 ng/mL) + 225RANKL287 (75 ng/mL), 158RANKL316 (75 ng/mL) + 225RANKL290 (75 ng/mL), 158RANKL316 (75 ng/mL) + 225RANKL292 (75 ng/mL), 158RANKL316 (75 ng/mL) + 225RANKL294 (75 ng/mL), and 158RANKL316 (75 ng/mL) + 225RANKL295 (75 ng/mL). Magnification, ×100; scale bar = 20 μm. (**d**) Quantification of TRAP-positive area; Data are presented as the mean ± SD of each data from independent measurements (n = 4). *p < 0.05 indicates a significant difference at 158RANKL316 vs. 225RANKL295. ns, not significant. SDS-PAGE, Sodium Dodecyl Sulfate-Polyacrylamide Gel Electrophoresis; IPTG, Isopropyl β-D-1-thiogalactopyranoside. The 3D simulations were created by Phyre2 (http://www.sbg.bio.ic.ac.uk/~phyre2/html/page.cgi?id=index) and quantified graph by GraphPad Prism 10 software (https://www.graphpad.com/).

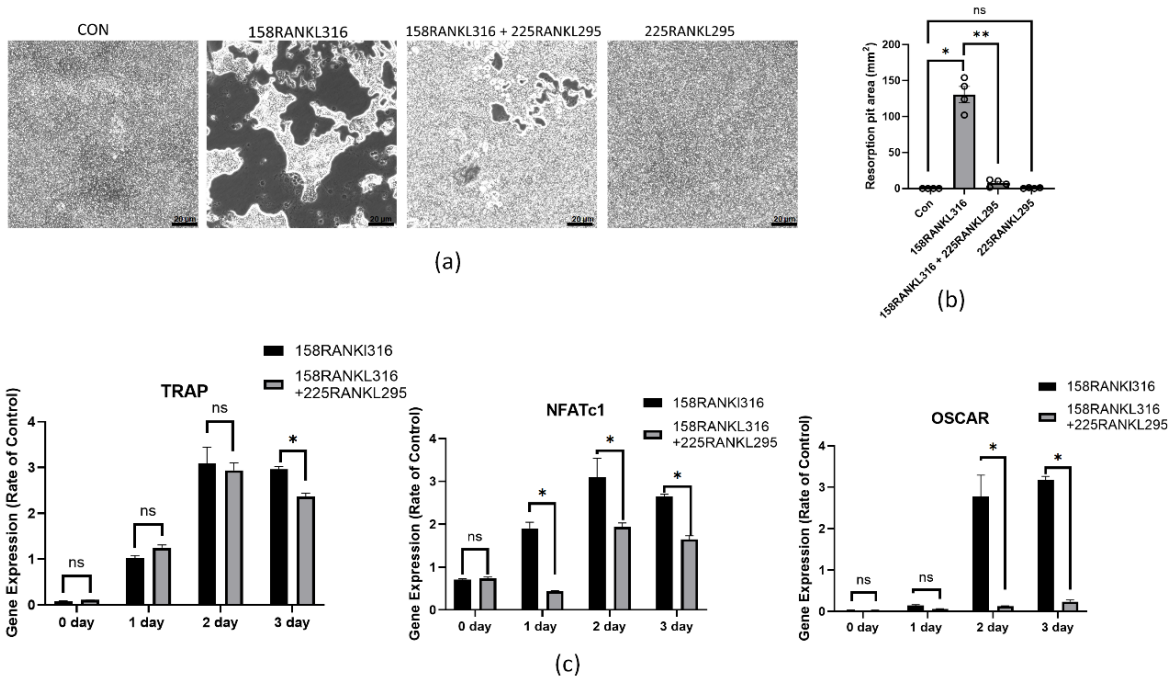

Fig. 3. Confirmation of the inhibition of osteoclast activation by RANKL-derived sequential fragment proteins. (**a**) Bone resorption pits were observed in Con, 158RANKL316, 158RANKL316 + 225RANKL295, and 225RANKL295-treated bone marrow-derived macrophages (BMMs). Magnification, ×100; scale bar = 20 μm. (**b**) Quantification of resorption pits. Data are presented as the mean ± SD of each data from independent measurements (n = 4). *$p < 0.05$ indicates a significant difference at Con vs. 158RANKL316 and **$p < 0.05$ at 158RANKL316 vs. 158RANKL316 + 225RANKL295. ns, not significant. (**c**) Expression of osteoclast-related genes in BMMs. BMMs were exposed to 158RANKL316 or 158RANKL316 + 225RANKL295 for 3 days. Data are presented as the mean ± SD of each data from independent measurements (n = 3). *$p < 0.01$ indicates a significant difference, respectively. ns, not significant. Con, control. The quantified graphs were created by GraphPad Prism 10 software (https://www.graphpad.com/).

(Nikon, ECLIPSE Ti2, Melville, NY, USA) and measured using Image J 1.52a software (National Institutes of Health, Bethesda, MD, USA).

Quantitative Real-Time Polymerase Chain Reaction (qRT-PCR) Procedure

The BMMs were cultured in six-well plates with M-CSF (30 ng/mL) and indicated small RANKL peptide (75 ng/mL) at 37.5 °C for designated durations (0, 1, 2 and 3 days). Total RNA was isolated using TRIzol® reagent (Invitrogen, 15596026, Thermo Fisher Scientific, Carlsbad, CA, USA), and complementary DNA (cDNA) was synthesized from 2 μg of RNA employing the ReverTra Ace qPCR RT Master Mix (FSQ-201, Toyobo Life Science, Osaka, Japan) in accordance with the supplier's instructions. Gene expression levels were subsequently assessed via real-time PCR. Glyceraldehyde-3-phosphate dehydrogenase (GAPDH) served as the internal normalization control. PCR reactions were carried out on the CFX Connect Real-Time PCR Detection System (SP71, Bio-Rad, Hercules, CA, USA) in a 20 μL volume containing 10 μL of iQ^{TM} SYBR® Green Supermix (1708880, Bio-Rad, Hercules, CA, USA), 10 pmol of each primer, and 1 μg of cDNA template. The sequences of primers for osteoclast differentiation were prepared according to previous research [25,26].

Measurement of the Binding Affinity

Binding affinity between ligand and receptor was measured by microscale thermophoresis (MST) as described previously [27]. For the binding check, as a receptor, RANK or LGR4, and RANKL ligands or indicated small RANKL peptide were mixed. The binding curves were determined using the manufacturer's protocol, and the Kd values were obtained from the mean of three replicates.

Western Blot Analysis

To investigate protein activation, cells were deprived of serum for 8 hours and subsequently stimulated with indicated small RANKL peptide (2 μg/mL) for 5, 15, or 30 minutes, respectively. Following stimulation, cells were harvested using 5× SDS sample buffer supplemented with protease and phosphatase inhibitor cocktails. Protein extracts (~ 30 mg) were resolved on 10 % Sodium Dodecyl Sulfate-Polyacrylamide Gel Electrophoresis (SDS-PAGE) gels and transferred onto polyvinylidene difluoride (PVDF) membranes (10600023, Amersham, Piscataway, NJ, USA). Membranes were blocked for 30 minutes at room

Table 1. Results of RANKL-based small fragment protein modeling using Phyre2.

Template	Template information	% Identification	Confidence
225RANKL282	TNF-like superfamily	100	97.2
225RANKL285	TNF-like superfamily	100	99.3
225RANKL287	TNF-like superfamily	100	99.3
225RANKL290	TNF-like superfamily	100	99.5
225RANKL292	TNF-like superfamily	100	99.5
225RANKL294	TNF-like superfamily	100	99.5
225RANKL295	TNF-like superfamily	100	99.5

RANKL, receptor activator of nuclear factor-kappa B ligand; TNF, tumor necrosis factor.

temperature in Tris buffered saline with 0.1 % Tween-20 (TBST) containing 5 % non-fat dry milk (Tris-Buffered Saline (TBS): 2.42 g/L Tris-HCl, 8 g/L NaCl; pH 7.6), then washed with TBST. Primary antibodies against p-AKT, AKT, p-GSK-3, GSK-3β, RANK, LGR4 and GAPDH were applied and incubated overnight at 4 °C according to previous study [25,26]. After washing, signal detection was performed using an enhanced chemiluminescence (ECL) system (Amersham, RPN3004, Slough, UK).

Separation of Nuclear and Cytoplasmic Fractions

To separate the nuclear and cytoplasmic fractions for NFATc1 detection, BMMs were prepared according to previous protocol [26]. The nuclear and cytosolic extracts were examined using western blot analysis. Histone-H1 and β-actin were used as loading controls, respectively.

In Vivo Experiment

A total of 20 female Balb/c mice (age, 5 weeks; weight, ~ 25 g; Orient Bio, Inc., Seongnam-si, Republic of Korea) were examined for *in vivo* experiment according to previous study [25,26]. The mice were randomly divided into four groups (n = 5/group) and the control groups were intraperitoneally injected with phosphate-buffered saline (PBS), those of 158RANKL316 group were injected with 158RANKL316 (1 mg/kg) in PBS, and those of 158RANKL316 + 225RANKL295 group were injected with 158RANKL316 (1 mg/kg) and 225RANKL295 (1 mg/kg) in PBS at 24 hours intervals for 2 days. The 225RANKL295 group was injected with 225RANKL295 (1 mg/kg in PBS). On day 3, after injection, all animals were euthanized with 50 % CO_2, and femur bone samples were acquired.

Microcomputed Tomography (Micro-CT) Scanning

The scanning of the distal femur by micro-CT was performed according to the method described previously [26] using a Quantum GX micro-CT imaging system (PerkinElmer, Inc., Waltham, MA, USA) at the Korea Basic Science Institute (Gwangju, Republic of Korea). The bone volume/tissue volume ratio (BV/TV), trabecular separation (Tb. Sp.), and bone mineral density (BMD) of the femur were analyzed and the values for the different parameters are presented as mean ± standard deviation (SD).

Histological Analysis of Mouse Tissue Samples

Mouse femurs were dissected, immersed in 4 % formaldehyde, and decalcified in 7 % ethylenediamine tetra-acetic acid (EDTA) for 30 days. After decalcifications, paraffine embed tissue sections were stained with hematoxylin and eosin (H&E) or TRAP, according to the method described previously [26].

Statistical Analyses

All *in vitro* and *in vivo* experiments were conducted at least in triplicate. All quantitative results are presented as mean ± SD. Primary comparisons of all experiments were carried out using a one-way analysis of variance with a Bonferroni multiple-comparisons test or unpaired Student's *t*-test. All statistical analyses were performed using GraphPad Prism, version 10 (GraphPad Inc., La Jolla, CA, USA).

Results

Classification of Small RANKL-Derived Peptides by RANK-Binding and Loop Region for Inhibition of Osteoclast Activation

The RANKL sequence encoded the 158 amino acid as a target region, which included residues 158–316 (Fig. 1**a**). In the present study, the RANKL active sites were classified according to their RANK-binding sites. Small protein fragments, in the 158–191, 191–225, and 225–316 amino acid regions, were synthesized, and their structures were determined via 3D simulation (Fig. 1**b**). Additionally, to analyze the suppressive effect of the synthesized protein fragments on osteoclast activity, TRAP staining was performed following treatment of BMMs with the synthesized protein containing the active site of RANKL (Fig. 1**c,d**). Treatment with the protein containing the active site of RANKL, 158RANKL316, increased the TRAP-positive multinucleated area. However, only 225RANKL316 had an inhibitory effect on the generation of TRAP-positive area in the presence of 158RANKL316.

Based on the above results, the 225–316 region of RANKL was reclassified into three subregions: 225RANKL244, which includes the βC-CD loop-βD region; 225RANKL260, which includes the βD-DE loop-βE region; and 225RANKL282, which includes the βE-EF loop-βF region. 225RANKL295, 225RANKL300, and 225RANKL316 were also identified as small-fragment

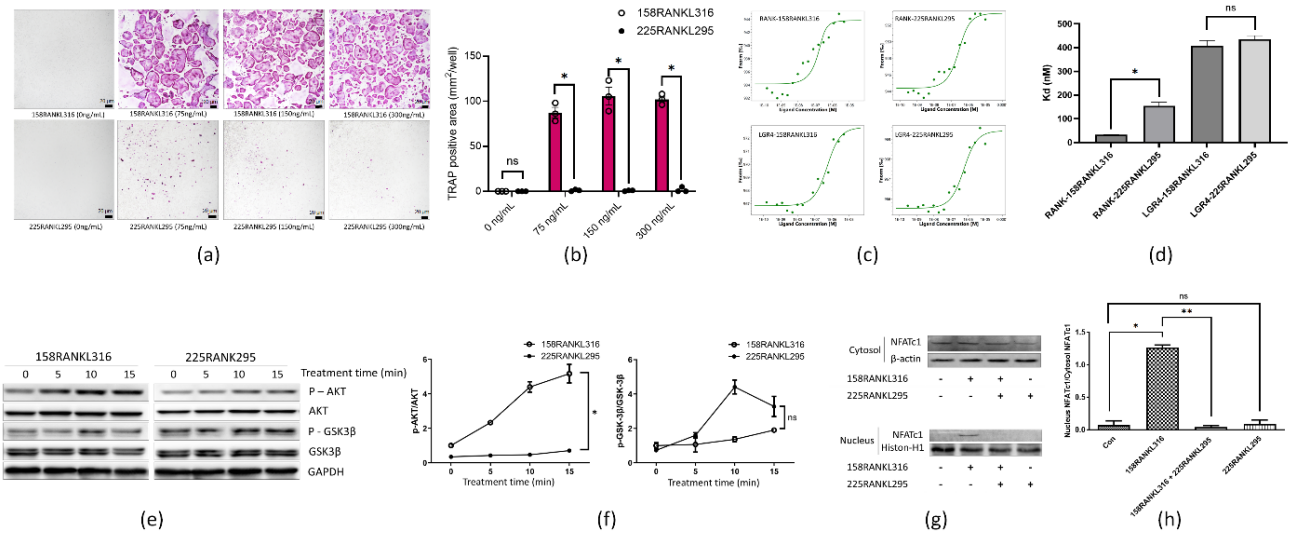

Fig. 4. Effect of RANKL-derived small fragment proteins on the LGR4 signaling cascade. (**a**) A representative image of BMMs stained for TRAP showing the dose-dependent effect of treatment with 158RANKL316 or 225RANKL295 on the generation of TRAP-positive multinucleated cells. Magnification ×100; scale bar = 20 μm. (**b**) Quantification of TRAP-positive area; Data are presented as the mean ± SD of each data from independent measurements (n = 3). *$p < 0.05$ indicates a significant difference at 158RANKL316 vs. 225RANKL295, respectevely. ns, not significant. (**c**) Concentration of 158RANKL316/225RANKL295 used in titration experiments, and the concentration of the labeled RANK and LGR4 was constant at 250 nM. The y-axis presents ligand-receptor affinity data using Frobenius normalization (F norm (%)). (**d**) Binding affinities (Kd values, dissociation constant) of RANK and LGR4 to 158RANKL316 and 225RANKL295. Data are presented as the mean ± SD from three independent experiments. *$p < 0.05$ indicates a significant difference at RANK-158RANKL316 vs. RANK-225RANKL295. ns, not significant. (**e**) Western blots of RANK and LGR4 signaling pathway proteins. GAPDH was used as a loading control. The results are representative of three separate experiments with comparable results. (**f**) Densitometric analysis of p-GSK-3β/GSK-3β and p-AKT/AKT determined. Data are presented as the mean ± SD of each data from three independent measurements (n = 3). *$p < 0.05$ indicates a significant difference at 158RANKL316 vs. 225RANKL295 at 15 minutes. ns, not significant. (**g**) Nuclear translocation of NFATc1 in 158RANKL316- or/and 225RANKL295-treated BMMs analyzed using cytoplasmic and nuclear fractions. (**h**) NFATc1 expressions in the nuclear and cytoplasmic fractions of 158RANKL316- or/and 225RANKL295-treated BMMs are presented as the mean ± standard deviation of three separate experiments. *$p < 0.05$ indicates a significant difference at Con vs. 158RANKL316 and **$p < 0.05$ at 158RANKL316 vs. 158RANKL316 + 225RANKL295, ns, not significant. LGR4, leucine-rich repeat containing G protein-coupled receptor 4; GAPDH, glyceraldehyde-3-phosphate dehydrogenase; GSK-3β, glycogen synthase kinase-3 beta; AKT, protein kinase B; NFATc1, nuclear factor of activated T cells. The quantified graphs were created by GraphPad Prism 10 software (https://www.graphpad.com/).

proteins. For selection, TRAP staining was performed in 158RANKL316-treated BMMs, and the TRAP-positive area was analyzed after treatment with each small fragment of RANKL (Fig. 1**e,f**). Only 225RANKL295, 225RANKL300, and 225RANKL316 significantly inhibited the TRAP activity. Therefore, the small fragment of RANKL from amino acid residue 225 was classified and synthesized into fragments 282–295 for further study.

Selection of RANKL-Derived Sequential Fragment Protein for Inhibition of Osteoclast Activation

To determine the minimum size of the RANKL-derived protein, small RANKL fragments, ranging from amino acid residues 225, 282, and 295, were synthesized. The expression of each small RANKL fragment was detected in SDS-PAGE gel (Fig. 2**a**). The recombinant proteins were purified using column chromatography. SDS-PAGE revealed about 19 kDa bands, matching the predicted size.

The 3D structural simulation model of each small RANKL fragment is shown in Fig. 2**b**. Protein models of 225RANKL290, 225RANKL292, 225RANKL294, and 225RANKL295 were generated using Phyre2 at confidence levels >99.5 %, despite their sequences being 100 % identical to the TNF superfamily (Table 1). To select the final candidates for osteoclast inhibition, BMMs treated with 225RANKL282, 225RANKL287, 225RANKL290, 225RANKL292, 225RANKL294, and 225RANKL295 in the presence of 158RANKL316 were subjected to TRAP staining (Fig. 2**c,d**). BMMs differentiated into multinucleated TRAP-positive osteoclasts, and the area was significantly higher for cells treated with 158RANKL316 alone. However, treatment with 225RANKL295 alone did not induce differentiation into TRAP-positive osteoclasts unlike

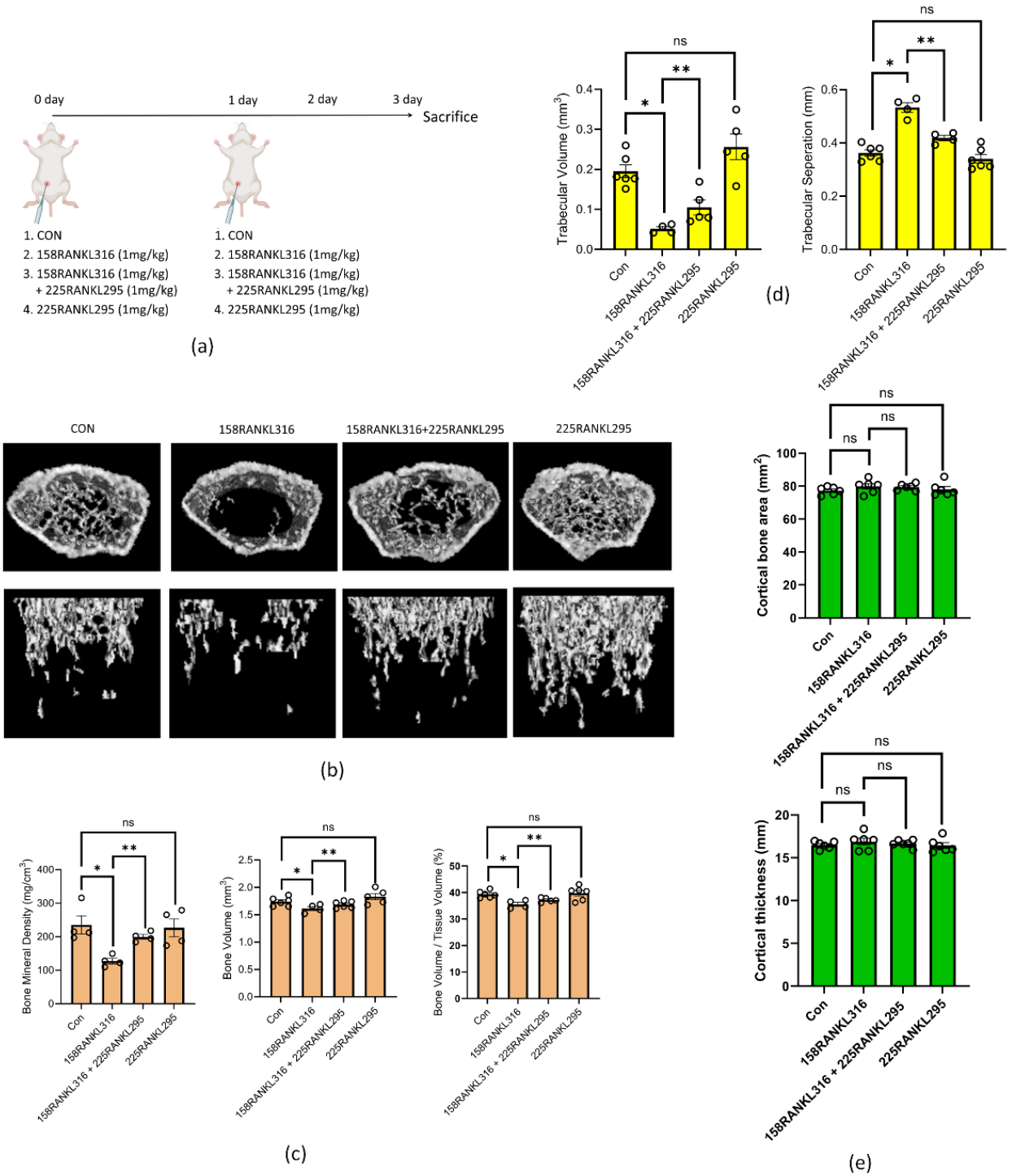

Fig. 5. Micro-CT analysis of RANKL-induced bone resorption. (**a**) Time schedule for treatment with the small RANKL fragment and sampling. (**b**) Micro-CT images revealed the trabecular bone architecture in the volume of interest in Con, 158RANKL316, 158RANKL316 + 225RANKL295, and 225RANKL295-treated mouse femur. (**c**) Bone mineral density (BMD), bone volume, bone volume/tissue volume are represented. (**d**) Trabecular seperations and trabecular bone volume. (**e**) Cortical bone area and cortical thickness. (**c–e**) Data are presented as the mean ± SD of each data from independent measurements (n = 5). *$p < 0.05$ compared with Con vs. 158RANKL316 and **$p < 0.05$ compared with 158RANKL316 vs. 158RANKL316 + 225RANKL295. ns, not significant. CT, computed tomography. The quantified graphs were created by GraphPad Prism 10 software (https://www.graphpad.com/).

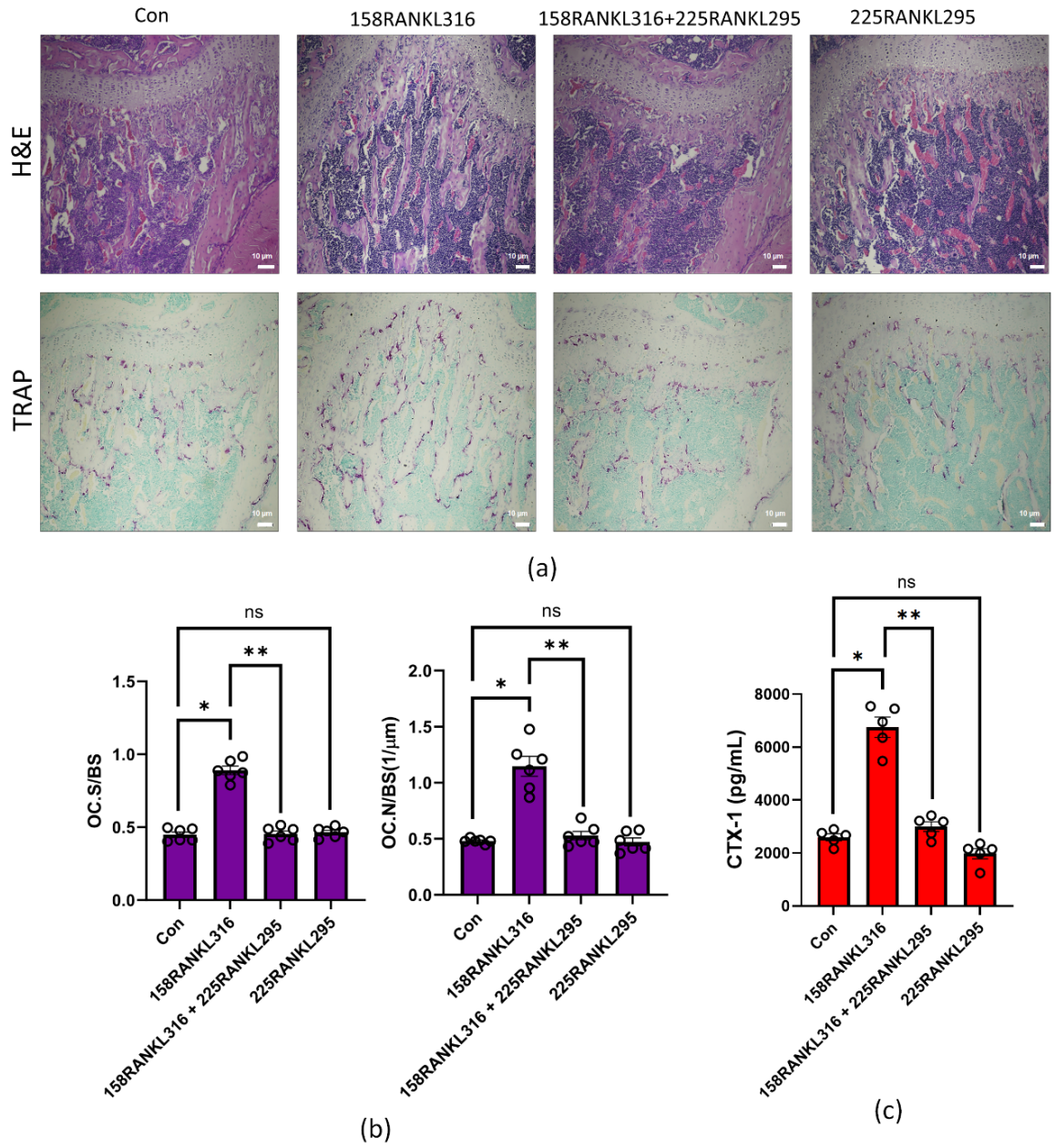

Fig. 6. Effect of RANKL-derived small fragment proteins on RANKL-induced bone resorption. (**a**) H&E and TRAP staining of mice femur. Magnification, ×200; scale bar = 10 μm. (**b**) Analysis of TRAP-positive osteoclast surface/bone surface. (**c**) CTX-1 level. (**b,c**) Data are presented as the mean ± SD of each data from independent measurements (n = 5). *$p < 0.05$ compared with Con vs. 158RANKL316 and **$p < 0.05$ compared with 158RANKL316 vs. 158RANKL316 + 225RANKL295. ns, not significant. H&E, hematoxylin and eosin; CTX-1, C-telopeptide of collagen type 1. The quantified graphs were created by GraphPad Prism 10 software (https://www.graphpad.com/).

that observed for other RANKL-derived small fragment proteins.

Confirmation of the Inhibition of Osteoclast Activation by RANKL-Derived Sequential Fragment Proteins

Bone resorption assays were performed to confirm the inhibitory effects of 225RANKL295 on osteoclast activity. Numerous resorption pits were observed in mature osteoclasts treated with 158RANKL316 (Fig. 3**a,b**). However, treatment with 225RANKL295 significantly decreased the area of resorption pits.

To elucidate the effect of 225RANKL295 signaling through the LGR4-involved pathway on osteoclastogenesis, we performed RT-PCR of osteoclast-specific genes, namely *TRAP*, *NFATc1*, and osteoclast-associated receptor (*OSCAR*), in BMMs treated with 158RANKL316 or/and

225RANKL295 (Fig. 3**c**). On day 3 post-treatment, the messenger ribonucleic acid (mRNA) expressions of *TRAP*, *NFATc1*, and *OSCAR*, which are markers of osteoclast differentiation and activity, were significant decreased in BMMs treated with 158RANKL316 and 225RANKL295 compared with the respective levels in 158RANKL316-treated cells. These results mean that 225RANKL295 can be a potential inhibitor of osteoclast activity.

Effect of RANKL-Derived Small Fragment Protein on the LGR4 Signaling Cascade

To clarify the effects of 225RANKL295 on the LGR4 signaling pathway, we examined TRAP activity in BMMs treated with 225RANKL295 alone. Treatment with 300 ng/mL 225RANKL295 did not affect the TRAP activity compared with 158RANKL316 (Fig. 4**a,b**).

We determined the binding affinities of 158RANKL316 and 225RANKL295 to RANK and LGR4 using the MST assay (Fig. 4**c,d**). The Kd binding value of 158RANKL316 with RANK was 33.3 ± 0.8 nM and that of 225RANKL295 with RANK was 154 ± 16 nM, meaning that the binding affinity of these small proteins for RANK was significant. The measured Kd value of active RANKL with RANK was 5-fold lower. However, the Kd value of 158RANKL316 with LGR4 (409 ± 21 nM) and of 225RANKL295 with LGR4 (436 ± 15 nM) was only slightly different. These results showed that 225RANKL295 could bind to LGR4, but not to RANK, unlike the active RANKL.

To investigate the effect of 225RANK295 on the LGR4 intracellur signaling pathway, we analyzed whether treatment of 158RANKL316 or 225RANKL295 leads the phosphorylated AKT and GSK-3β through the RANK and LGR4 signaling pathway (Fig. 4**e,f**). The 225RANKL295 treatment induced an apparent increase in phosphorylation of GSK-3β and a decrease in phosphorylation of AKT, compared with that in the 158RANKL316 treatment.

To investigate the effect of 225RANKL295 on the LGR4-induced inhibition of NFATc1 translocation to nucleus, the nucleus and cytosolic NFATc1 levels were analyzed (Fig. 4**g,h**). NFATc1 in nucleus fraction of 225RANKL295-treated BMMs was not detected in the presence of 158RANKL316. This finding suggests that 225RANK295 may stimulate GSK-3β phosphorylation through the LGR4 signaling pathway without activating the canonical signaling of RANK.

Effect of RANKL-Derived Small Fragment Protein on RANKL-Induced Bone Resorption

To elucidate the effects of 225RANKL295 on bone resorption, we administered 158RANKL316 and 225RANKL295 to healthy mice. Femoral trabecular and cortical bones were then analyzed using by micro-CT (Fig. 5**a**). Mice treated with 158RANKL316 developed mild osteoporosis, as evidenced by significant reduction in BMD, bone volume, and BV/TV (Fig. 5**b,c**). However, treatment with 225RANKL295 led to an obvious inhibition of 158RANKL316-induced osteoporotic bone resorption in mice. Furthermore, it significantly improved BMD, bone volume, and BV/TV and there was no significance in the values of these parameters between control and 225RANKL295-treated mice. Micro-CT analysis of the mouse femur showed that 158RANKL316 affected osteolysis. However, 225RANKL295 alone did not have any impact on osteoclast differentiation. Trabecular bones in the 158RANKL316-induced mice femur treated with 225RANKL295 were apparently significantly thicker and denser than those from untreated 158RANKL316-induced mice. The trabecular bone volume in the control group (0.187 ± 0.02 mm^3) and in the group of 158RANKL316-induced mice treated with 225RANKL295 (0.123 ± 0.09 mm^3) was higher than that in the mice induced by 158RANKL316 alone (0.031 ± 0.001 mm^3, both $p < 0.05$), significantly (Fig. 5**d**). Trabecular separation in control and 225RANKL295-treated mice was also lower than that in 158RANKL316-induced mice, significantly. In contrast, treatment with 158RANKL316 did not showed significantly in the cortical bone area or cortical thickness, and no significant change was noted upon treatment with 225RANKL295 (Fig. 5**e**). These results showed that the administration of 225RANKL295 to active RANKL-treated mice significantly recovered bone resorption and was particularly effective in suppressing the resorption of the trabecular bone.

Effect of RANKL-Derived Small Fragment Protein on the Activity of Osteoclast in RANKL-Induced Mice

To elucidate the effect of small-fragment proteins derived from RANKL on the inhibition of osteoclast activity, we analyzed the TRAP-positive osteoclasts number and surface area in the femur of mice treated with 158RANKL316 (Fig. 6**a–c**). Mice treated with 158RANKL316 showed an increase of the TRAP-positive osteoclasts numbers in femur sections. However, 225RANKL295 treatment led to a significant decrease in area and number of TRAP-positive surfaces. Therefore, 225RANKL295 has the potential to inhibit RANKL-induced bone resorption by inhibiting osteoclast activity in mouse models.

Discussion

Over the past few decades, therapeutic approaches targeting RANKL have been tried to be effective for osteoporosis treatment. Osteoprotegerin (OPG)-Fc, which was originally identified as a RANK decoy receptor, was designed as an inhibitor of RANKL [28]. These variants significantly reduce osteoclastogenesis [29]. In addition to OPG-Fc, several recombinant proteins targeting RANKL have been developed as potential interventions to reduce bone loss in osteoporosis [30]. One such pro-

tein, denosumab (Prolia), was approved by the U.S. Food and Drug Administration (FDA) as a therapeutic agent for bone loss in osteoporosis as well as for the management of bone metastatic cancer. Denosumab acts as a scavenger of RANKL and effectively inhibits the RANKL-RANK pathway [31]. Despite their notable medical and commercial success, antibody agents, including OPG-Fc and denosumab, have raised concerns owing to their limited half-lives and potential immunogenicity. These challenges include manufacturing complexities, exorbitant treatment expenses, patient adherence to regular injection schedules, and limited effectiveness, as evidenced in numerous reports [32,33]. Consequently, in comparison with antibodies and other biologics, the use of small protein fragments such as peptides presents a more favorable approach for managing chronic diseases [34]. This is because of their distinct advantages, including cost-effectiveness, reduced immunogenicity, and minimal protein dosage required to elicit a therapeutic response [35]. Therefore, the development of treatment targeting LGR4 can be a viable and novel therapeutic strategy for osteoporosis treatment. LGR4 was recently identified as an additional receptor for RANKL [21]. This newly discovered RANKL receptor for binding to RANKL competes with RANK, thereby, inhibiting canonical RANK-NFATc1 signaling and osteoclast activation [26]. LGR4 signal compensates the RANKL-induced osteoclast activation [26]. This inhibition occurs through the blocking of signaling pathways derived from RANK-TNF receptor-associated factor (TRAF)6 and the inactivation of GSK-3β, which is necessary for osteoclast activation.

To demonstrate this concept in the present study, a small RANKL-derived fragment was used to initiate LGR4 signaling. This small-fragment protein was synthesized using the RANKL sequence and exhibited a structure closely resembling that of the original RANKL. A specific small fragment, 225RANKL295, did not exhibit a significant difference in LGR4 binding affinity. Both *in vitro* and *in vivo* study showed that treatment with the small RANKL fragment effectively hindered differentiation and activation of osteoclast in the presence of active RANKL, suggesting that the small RANKL fragment may function as a compensation of RANKL, acting as an LGR4 agonist. According to our previous research, the LGR4 agonist activates the GSK-3β signaling pathways and inhibits nucleus translocation of NFATc1 during osteoclast differentiation [27]. In the LGR4 small interfering ribonucleic acid (siRNA) treated cells, GSK-3β signaling was not observed and NFATc1 translocation was detected in presence or absence of LGR4 agonist in RANKL-induced BMMs [27]. These data provide the evidence that LGR4 can play a trigger role in the negative feedback mechanism for regulation of osteoclast activity. The stimulation of LGR4 signal in pre-osteoclasts can initiate a negative regulatory signaling pathway that surpasses the canonical RANK signaling and subsequently inhibits NFATc1-involved pathway. Luo *et al*. [21] announced that the LGR4 extracellular domain could play a role of a decoy receptor, effectively binding to RANKL. This interaction subsequently hindered RANKL-induced osteoclastogenesis [21].

Recently, advances have been made in devising potential therapeutic approaches targeting RANKL; these include the development of antibodies and vaccines [36]. Compared with other biologics, peptides can offer a more favorable strategy for therapeutics owing to their distinct advantages, including cost-effectiveness and the ability to induce the desired effect with small protein doses [37,38]. Therefore, the current approach, which employs the targeted integration of an immunogen, may serve as a viable solution to circumvent these challenges. Further investigations on the safety, stability in physiological environment and significance of the peptide-sized proteins as well as on any discernible adverse effects of immunization are necessary as a long-term study. The present study had limitations regarding the detection of bone remodeling and osteoblast markers, including alkaline phosphatase (ALP) levels, as well as the lack of histological evidence of bone remodeling. In addition, investigation of the downstream molecular events and signaling transduction cascade is required to elucidate the effect of this present peptide on LGR4-GSK-3β-NFATc1 pathway. Furthermore, it is imperative to investigate the human RANKL-derived peptides in human RANKL knock-ins to assess the clinical applicability of this RANKL-derived peptide.

Conclusions

In this study, we showed that 225RANKL295, a small fragment derived from RANKL based on its protein structure was able to bind to LGR4 but not to RANK. Treatment with 225RANKL295 resulted in the GSK-3β phosphorylation and the inhibition of TRAP and osteoclast activity in bone marrow-derived macrophages. This treatment also led to the inhibition of bone resorption in the femur of RANKL-treated mice. Our results offer empirical support for the potential use of the RANKL fragment as a therapeutic intervention for osteoporosis. The RANKL fragment inhibited RANKL-induced osteoclastogenesis, and this inhibition was counterbalanced by RANKL inhibition. This study suggests that the RANKL-derived small protein provides a promising avenue for the advancement of novel therapeutic approaches to treat osteoporosis.

List of Abbreviations

OPG, osteoprotegerin; RANK, receptor activator of nuclear factor-kappa B; RANKL, RANK ligand; TRAP, tartrate-resistant acid phosphatase; TNF, tumor necrosis factor; MAPK, mitogen-activated protein kinase; NF-κB, nuclear factor-kappa B; NFATc1, nuclear factor of activated T cells; 3D, three dimensional; TRAFs, TNF receptor-associated factors; GSK-3β, glycogen synthase

kinase-3 beta; cDNA, complementary deoxyribonucleic acid; BMMs, bone marrow-derived macrophages; OSCAR, osteoclast-associated receptor; GAPDH, glyceraldehyde-3-phosphate dehydrogenase; RT-PCR, real-time polymerase chain reaction; MST, microscale thermophoresis; CT, computed tomography; BV, bone volume; TV, tissue volume; Tb. Sp., trabecular separation; BMD, bone mineral density; SD, standard deviation; EDTA, ethylenediamine tetra-acetic acid; H&E, hematoxylin and eosin; M-CSF, macrophage-colony stimulation factor; PBS, phosphate-buffered saline; LGR4, leucine-rich repeat containing G protein-coupled receptor 4; α-MEM, α-minimal essential medium; TBST, Tris buffered saline with 0.1 % Tween-20; AKT, protein kinase B; SDS-PAGE, Sodium Dodecyl Sulfate-Polyacrylamide Gel Electrophoresis; IPTG, Isopropyl β-D-1-thiogalactopyranoside; Con, control; CTX-1, C-telopeptide of collagen type 1.

Availability of Data and Materials

All requests for raw and analyzed data and materials will be promptly reviewed to verify whether the request is subject to any intellectual property or confidentiality obligations by the corresponding author and Chosun University, Republic of Korea.

Author Contributions

YJ, YJC and WL contributed to the design of this work. YJ and YJC performed cell culture, basic analysis and animal experiments. YK and HL performed the generation, purification of peptide and MST analysis. BK contributed TRAP staining, real-time PCR and western blot analysis. CML was responsible for statistical analysis and contributed to the animal study. YJ, YJC, YK, HL, BK, CML and WL contributed to the interpretation of data. YJ, YJC and WL drafted the work. YK, HL, BK and CML contributed to draft the work. YJ, YJC and WL revised critically for important intellectual content. All authors read and approved the final manuscript. All authors agreed to be accountable for all aspects of the work in ensuring that questions related to the accuracy or integrity of any part of the work were appropriately investigated and resolved.

Ethics Approval and Consent to Participate

All animal experiments were carried out in compliance with institutional and governmental requirements approved by the Institutional Animal Care and Use Committee (approval no. CIACUC2021-S0007) of Chosun University, Gwangju, Republic of Korea.

Acknowledgments

The graphical abstract was created in BioRender. https://BioRender.com/h23j566.

Funding

This study was supported by the National Research Foundation of Korea (NRF) and was funded by the Korean government (NRF-2022R1A2C2009119, NRF-2021R1I1A3046499, and RS-2023-00217471).

Conflict of Interest

The authors declare they have no conflicts of interest.

Supplementary Material

Supplementary material associated with this article can be found, in the online version, at https://doi.org/10.22203/eCM.v053a02.

References

[1] Shin HR, Kim BS, Kim HJ, Yoon H, Kim WJ, Choi JY, *et al*. Excessive osteoclast activation by osteoblast paracrine factor RANKL is a major cause of the abnormal long bone phenotype in Apert syndrome model mice. Journal of Cellular Physiology. 2022; 237: 2155–2168. https://doi.org/10.1002/jcp.30682.

[2] Azuma Y, Kaji K, Katogi R, Takeshita S, Kudo A. Tumor necrosis factor-alpha induces differentiation of and bone resorption by osteoclasts. The Journal of Biological Chemistry. 2000; 275: 4858–4864. https://doi.org/10.1074/jbc.275.7.4858.

[3] Boyce BF, Xing L. Functions of RANKL/RANK/OPG in bone modeling and remodeling. Archives of Biochemistry and Biophysics. 2008; 473: 139–146. https://doi.org/10.1016/j.abb.2008.03.018.

[4] Zauli G, Rimondi E, Nicolin V, Melloni E, Celeghini C, Secchiero P. TNF-related apoptosis-inducing ligand (TRAIL) blocks osteoclastic differentiation induced by RANKL plus M-CSF. Blood. 2004; 104: 2044–2050. https://doi.org/10.1182/blood-2004-03-1196.

[5] Huang H, Chang EJ, Ryu J, Lee ZH, Lee Y, Kim HH. Induction of c-Fos and NFATc1 during RANKL-stimulated osteoclast differentiation is mediated by the p38 signaling pathway. Biochemical and Biophysical Research Communications. 2006; 351: 99–105. https://doi.org/10.1016/j.bbrc.2006.10.011.

[6] Ma C, Mo L, Wang Z, Peng D, Zhou C, Niu W, *et al*. Dihydrotanshinone I attenuates estrogen-deficiency bone loss through RANKL-stimulated NF-κB, ERK and NFATc1 signaling pathways. International Immunopharmacology. 2023; 123: 110572. https://doi.org/10.1016/j.intimp.2023.110572.

[7] Tomomura M, Hasegawa H, Suda N, Sakagami H, Tomomura A. Serum calcium-decreasing factor, caldecrin, inhibits receptor activator of NF-κB ligand (RANKL)-mediated Ca2+ signaling and actin ring formation in mature osteoclasts via suppression of Src signaling pathway. The Journal of Biological Chemistry. 2012; 287: 17963–17974. https://doi.org/10.1074/jbc.M112.358796.

[8] Lee K, Chung YH, Ahn H, Kim H, Rho J, Jeong D. Selective Regulation of MAPK Signaling Mediates RANKL-dependent Osteoclast Differentiation. International Journal of Biological Sciences. 2016; 12: 235–245. https://doi.org/10.7150/ijbs.13814.

[9] Huang H, Ryu J, Ha J, Chang EJ, Kim HJ, Kim HM, *et al*. Osteoclast differentiation requires TAK1 and MKK6 for NFATc1 induction and NF-kappaB transactivation by RANKL. Cell Death and Differentiation. 2006; 13: 1879–1891. https://doi.org/10.1038/sj.cdd.4401882.

[10] Burgess TL, Qian Y, Kaufman S, Ring BD, Van G, Capparelli C, *et al*. The ligand for osteoprotegerin (OPGL) directly activates mature osteoclasts. The Journal of Cell Biology. 1999; 145: 527–538. https://doi.org/10.1083/jcb.145.3.527.

[11] Itzstein C, Coxon FP, Rogers MJ. The regulation of osteoclast function and bone resorption by small GTPases. Small GTPases. 2011; 2: 117–130. https://doi.org/10.4161/sgtp.2.3.16453.

[12] Lo Iacono N, Blair HC, Poliani PL, Marrella V, Ficara F, Cassani B, *et al*. Osteopetrosis rescue upon RANKL administration to Rankl(-/-) mice: a new therapy for human RANKL-dependent ARO. Journal of Bone and Mineral Research: The Official Journal of the American Society for Bone and Mineral Research. 2012; 27: 2501–2510. https://doi.org/10.1002/jbmr.1712.

[13] Lam J, Nelson CA, Ross FP, Teitelbaum SL, Fremont DH. Crystal structure of the TRANCE/RANKL cytokine reveals determinants of receptor-ligand specificity. The Journal of Clinical Investigation. 2001; 108: 971–979. https://doi.org/10.1172/JCI13890.

[14] Nelson CA, Warren JT, Wang MW, Teitelbaum SL, Fremont DH. RANKL employs distinct binding modes to engage RANK and the osteoprotegerin decoy receptor. Structure. 2012; 20: 1971–1982. https://doi.org/10.1016/j.str.2012.08.030.

[15] Luan X, Lu Q, Jiang Y, Zhang S, Wang Q, Yuan H, *et al*. Crystal structure of human RANKL complexed with its decoy receptor osteoprotegerin. The Journal of Immunology: Official Journal of the American Association of Immunologists. 2012; 189: 245–252. https://doi.org/10.4049/jimmunol.1103387.

[16] Locksley RM, Killeen N, Lenardo MJ. The TNF and TNF receptor superfamilies: integrating mammalian biology. Cell. 2001; 104: 487–501. https://doi.org/10.1016/s0092-8674(01)00237-9.

[17] Park JH, Lee NK, Lee SY. Current Understanding of RANK Signaling in Osteoclast Differentiation and Maturation. Molecules and Cells. 2017; 40: 706–713. https://doi.org/10.14348/molcells.2017.0225.

[18] Takayanagi H, Kim S, Matsuo K, Suzuki H, Suzuki T, Sato K, *et al*. RANKL maintains bone homeostasis through c-Fos-dependent induction of interferon-beta. Nature. 2002; 416: 744–749. https://doi.org/10.1038/416744a.

[19] Jin Y, Yang Y. LGR4: A new receptor for a stronger bone. Science China. Life Sciences. 2016; 59: 735–736. https://doi.org/10.1007/s11427-016-5068-8.

[20] Yue Z, Niu X, Yuan Z, Qin Q, Jiang W, He L, *et al*. RSPO2 and RANKL signal through LGR4 to regulate osteoclastic premetastatic niche formation and bone metastasis. The Journal of Clinical Investigation. 2022; 132: e144579. https://doi.org/10.1172/JCI144579.

[21] Luo J, Yang Z, Ma Y, Yue Z, Lin H, Qu G, *et al*. LGR4 is a receptor for RANKL and negatively regulates osteoclast differentiation and bone resorption. Nature Medicine. 2016; 22: 539–546. https://doi.org/10.1038/nm.4076.

[22] Lim W. LGR4 (GPR48): The Emerging Inter-Bridge in Osteoimmunology. Biomedicines. 2025; 13: 607. https://doi.org/10.3390/biomedicines13030607.

[23] Matsumoto Y, Larose J, Kent OA, Lim M, Changoor A, Zhang L, *et al*. RANKL coordinates multiple osteoclastogenic pathways by regulating expression of ubiquitin ligase RNF146. The Journal of Clinical Investigation. 2017; 127: 1303–1315. https://doi.org/10.1172/JCI90527.

[24] Ordaz-Ramos A, Rosales-Gallegos VH, Melendez-Zajgla J, Maldonado V, Vazquez-Santillan K. The Role of LGR4 (GPR48) in Normal and Cancer Processes. International Journal of Molecular Sciences. 2021; 22: 4690. https://doi.org/10.3390/ijms22094690.

[25] Jang Y, Sohn HM, Ko YJ, Hyun H, Lim W. Inhibition of RANKL-Induced Osteoclastogenesis by Novel Mutant RANKL. International Journal of Molecular Sciences. 2021; 22: 434. https://doi.org/10.3390/ijms22010434.

[26] Ko YJ, Sohn HM, Jang Y, Park M, Kim B, Kim B, *et al*. A novel modified RANKL variant can prevent osteoporosis by acting as a vaccine and an inhibitor. Clinical and Translational Medicine. 2021; 11: e368. https://doi.org/10.1002/ctm2.368.

[27] Jang Y, Lee H, Cho Y, Choi E, Jo S, Sohn HM, *et al*. An LGR4 agonist activates the GSK-3β pathway to inhibit RANK-RANKL signaling during osteoclastogenesis in bone marrow-derived macrophages. International Journal of Molecular Medicine. 2024; 53: 10. https://doi.org/10.3892/ijmm.2023.5334.

[28] Body JJ, Greipp P, Coleman RE, Facon T, Geurs F, Fermand JP, *et al.* A Phase I study of AMGN-0007, a recombinant osteoprotegerin construct, in patients with multiple myeloma or breast carcinoma related bone metastases. Cancer. 2003; 97: 887–892. https://doi.org/10.1002/cncr.11138.

[29] Higgs JT, Jarboe JS, Lee JH, Chanda D, Lee CM, Deivanayagam C, *et al.* Variants of Osteoprotegerin Lacking TRAIL Binding for Therapeutic Bone Remodeling in Osteolytic Malignancies. Molecular Cancer Research: MCR. 2015; 13: 819–827. https://doi.org/10.1158/1541-7786.MCR-14-0492.

[30] Ta HM, Nguyen GT, Jin HM, Choi J, Park H, Kim N, *et al*. Structure-based development of a receptor activator of nuclear factor-kappaB ligand (RANKL) inhibitor peptide and molecular basis for osteopetrosis. Proceedings of the National Academy of Sciences of the United States of America. 2010; 107: 20281–20286. https://doi.org/10.1073/pnas.1011686107.

[31] Liu C, Zhao Y, He W, Wang W, Chen Y, Zhang S, *et al*. A RANKL mutant used as an inter-species vaccine for efficient immunotherapy of osteoporosis. Scientific Reports. 2015; 5: 14150. https://doi.org/10.1038/srep14150.

[32] Krishna M, Nadler SG. Immunogenicity to Biotherapeutics-The Role of Anti-drug Immune Complexes. Frontiers in Immunology. 2016; 7: 21. https://doi.org/10.3389/fimmu.2016.00021.

[33] Lloyd SA, Morony SE, Ferguson VL, Simske SJ, Stodieck LS, Warmington KS, *et al.* Osteoprotegerin is an effective countermeasure for spaceflight-induced bone loss in mice. Bone. 2015; 81: 562–572. https://doi.org/10.1016/j.bone.2015.08.021.

[34] AlDeghaither D, Smaglo BG, Weiner LM. Beyond peptides and mAbs–current status and future perspectives for biotherapeutics with novel constructs. Journal of Clinical Pharmacology. 2015; 55: S4–S20. https://doi.org/10.1002/jcph.407.

[35] Achilleos K, Petrou C, Nicolaidou V, Sarigiannis Y. Beyond Efficacy: Ensuring Safety in Peptide Therapeutics through Immunogenicity Assessment. Journal of Peptide Science: an Official Publication of the European Peptide Society. 2025; 31: e70016. https://doi.org/10.1002/psc.70016.

[36] Wu T, Li F, Sha X, Li F, Zhang B, Ma W, *et al*. A novel recombinant RANKL vaccine prepared by incorporation of an unnatural amino acid into RANKL and its preventive effect in a murine model of collagen-induced arthritis. International Immunopharmacology. 2018; 64: 326–332. https://doi.org/10.1016/j.intimp.2018.09.022.

[37] Barman P, Joshi S, Sharma S, Preet S, Sharma S, Saini A. Strategic Approaches to Improvise Peptide Drugs as Next Generation Therapeutics. International Journal of Peptide Research and Therapeutics. 2023; 29: 61. https://doi.org/10.1007/s10989-023-10524-3.

[38] Wang L, Wang N, Zhang W, Cheng X, Yan Z, Shao G, *et al*. Therapeutic peptides: current applications and future directions. Signal Transduction and Targeted Therapy. 2022; 7: 48. https://doi.org/10.1038/s41392-022-00904-4.

Editor's note: The Scientific Editor responsible for this paper was Juerg Gasser.

Received: 15th November 2024; **Accepted**: 30th June 2025; **Published**: 30th September 2025